THE DEVELOPMENT AND STRUCTURE OF NOCTURNAL SLOPE WINDS IN A SIMPLE VALLEY[1]

J. C. DORAN, T. W. HORST and C. D. WHITEMAN

Pacific Northwest Laboratory, P.O. Box 999, Richland, Washington 99352, U.S.A.

(Received in final form 10 November, 1989)

Abstract. The results of an observational and modeling study of the nocturnal slope winds in a simple valley are presented. The valley was approximately 225 m deep in the region of the measurements, and featured a uniform slope angle of approximately 23° on one of its sidewalls. The wind and temperature structure of the katabatic flows on the valley sidewalls were measured with tower-mounted instruments, and a Doppler sodar and instruments on a tethered balloon and a 61-m tower were used to determine the atmospheric conditions near the center of the valley. The temperature structure of the slope flows was summarized by characteristic scale parameters h and ΔT for the inversion depth and strength, respectively. On the sidewalls 50 m above the valley floor, the inversion depths were generally smaller and the inversion strengths were weaker than they were on the sidewalls 100 m higher. These results differ significantly from those obtained over a simple slope of an isolated mountain or ridge. The down-valley winds are shown to be important in limiting the strength of the sidewall inversions. The formation of an inversion in the valley also has a pronounced effect on the structure of the slope flows. Numerical simulations suggest that the presence of adiabatic layers in the valley atmosphere is associated with decreases in the slope-flow inversion depth with increasing downslope distance. The simulations also indicate that the length scales that characterize the momentum and inversion depths behave similarly in flows down simple slopes but not in flows down the sidewalls of a valley.

1. Introduction

This paper describes an observational and modeling study of the nocturnal drainage flows that form on the sidewalls of a simple valley. We wished to compare and contrast the development and structure of katabatic flows over a valley sidewall to that found over a simple slope (Doran and Horst, 1983; Horst and Doran, 1986, 1988). Over a simple slope on Rattlesnake Mountain in eastern Washington, the inversion depth and the product of the inversion depth and inversion strength had been found to increase with increasing downslope distance. There was usually, but not always, a corresponding increase in the maximum downslope wind speed, the height of the wind speed maximum, and the general depth of the downslope flow. The change in the strength of the inversion with downslope distance was generally minor, however, and had no consistent sign.

Based on these observations, a simple conceptual picture was developed for some of the features of slope flows expected in a simple valley. Katabatic winds form over a slope in response to the temperature difference between the cooled air in the vicinity of the slope and the warmer air found at the same elevation but

[1]Work supported by the U.S. Army Research Office under Contract DA-AG29-K-0231 and the U.S. Department of Energy under Contract DE-AC06-76RLO 1830.

Boundary-Layer Meteorology **52**: 41–68, 1990.

farther from the slope. While a local inversion forms over a valley sidewall, a downslope wind develops there. However, an inversion also forms over the valley floor, and while this inversion deepens, more of the sidewalls will be contained within this cold layer. The local inversions on the sidewalls should then weaken in these regions, so that the katabatic winds should also become weaker. Moreover, as the along-valley winds increase, the winds on the slopes should turn more toward the down-valley direction. This picture proved to be an incomplete one, as will be described in this paper.

Our discussion begins in Section 2 with a description of the field site and the layout of the various instruments that were deployed. Section 3 presents a brief description of the synoptic conditions in which the experiments were conducted as well as a summary of the structure and evolution of the wind and temperature fields in the center of the valley. The valley meteorology determines the ambient conditions within which the slope flows develop and plays a major role in determining the slope flow behavior. Section 4 discusses the structure of the katabatic flows on the valley sidewalls. The discussion includes descriptions of the strengths and depths of the inversions that form over the slopes and descriptions of some of the characteristics of the katabatic winds. Section 5 describes the time-varying behavior of slope flow features and their relationship to the changing meteorology in the valley. The similarities and differences in the behaviour of slope flows over simple slopes and over valley sidewalls are also summarized. A numerical model was used to study further some features of the slope winds, and these studies are described in Section 6. Numerical simulations were used to examine the influence of the structure of the valley inversion in determining the downslope evolution of the slope flows. They also clarify the difference between inversion and momentum length scales for the slope flows and how these scales are related to each other over simple slopes and over valley sidewalls.

2. Site Description and Instrumentation

A valley in southeastern Washington was selected for our study site. The valley lies near the town of Dayton and was formed by the South Fork of the Touchet River as it flows out of the Blue Mountains. Figure 1 shows a topographical map of the area where the measurements were made. In this area, the valley is approximately 225 m deep, and runs from southeast to northwest. Within the study area, the valley is straight and contains no major tributaries, although a 45° bend occurs about 2 km upvalley. The east sidewall in our study area has a section of particularly uniform slope angle that extends for about 1.5 km along the valley and over most of the vertical extent from the ridgeline to the valley floor. The slope angle is approximately 23°, except for the lowest portions of the slope where the angle increases to about 40°. The vegetation consists primarily of dry grasses; trees are found near the river on the valley floor but do not extend up the sidewall.

Three 9-m towers were located on the east sidewall at the positions labeled A,

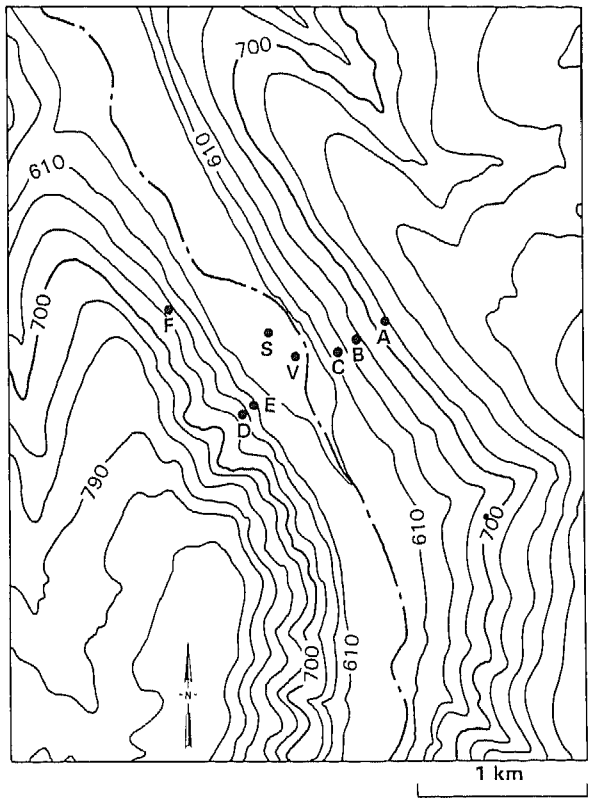

Fig. 1. Topographic map of measurement sites. Locations of Towers A through F are shown. S: sodar; V: 61-m tower. Contour heights are in meters. The dashed line marks the south fork of the Touchet River.

B, and C in Figure 1. The base elevations of the towers were nominally 50, 100, and 150 m above the valley floor, and the towers were all located on the section of the slope with a nearly constant slope angle. Thermocouples measured the temperature at six levels on each of the towers, and three-component propeller anemometers measured the wind velocity at three levels. Net radiation was also recorded at each of the towers. All data were sampled at 2-s intervals and averaged for periods of 2 min. The highest anemometer at tower A was located at a lower height than the corresponding instuments at towers B and C because the measurements over simple slopes suggested that the katabatic layer would be shallower at tower A.

Three additional 9-m towers, labeled D, E, and F, were placed on the west sidewall. Table I lists the instrument heights at each of the towers. The west sidewall is considerably more convoluted than the east sidewall, and portions of it are covered with low bushes and some trees. Because the east sidewall is much more regular in its slope angle and because its vegetation is much simpler, this

TABLE I

Heights of temperature (T) and wind (W) sensors on sidewall and valley towers

Tower	Height above valley floor (m)	Sensor	Sensor height (m)
A	147	T	0.18, 0.61, 1.35, 2.82, 5.74, 8.99
		W	0.66, 1.47, 3.51
B	99	T	0.13, 0.56, 1.35, 2.79, 5.87, 8.94
		W	0.74, 1.46, 6.00
C	52	T	0.18, 0.58, 1.35, 2.85, 5.89, 8.94
		W	0.63, 1.47, 5.89
D	92	T	0.11, 0.48, 1.40, 2.90, 5.94, 8.61
E	52	T	0.11, 0.45, 1.21, 2.73, 5.73, 8.67
		W	1.52, 3.09, 5.92
F	88	T	0.11, 0.58, 1.35, 2.95, 5.99, 8.89
		W	0.74, 1.35, 5.99
V	0	T	7.62, 17.1, 32.3, 47.5, 62.4
		W	3.05, 7.62, 17.4, 32.7, 47.9, 63.1

paper has been limited primarily to the analysis of the data collected from towers A, B, and C.

A 61-m tower (V in Table I) was erected on the valley floor to record wind and temperature profiles at the tower levels within the valley. The tower had six levels of three-component propeller anemometers for wind measurement and five levels of thermistors for temperature measurement. A three-component Doppler sodar was used to record the winds over the center of the valley over a height range of 50 to ~400 m. Doppler data were collected over 25-m range gates and averaged over 10-min time intervals.

During the evening transition periods, an instrument package was flown on a tethered balloon (Tethersonde®, Atmospheric Instrumentation Research, Inc., Boulder, Colorado) near tower V to record the temperature structure in the center of the valley and above the ridge tops. The balloon data collection system also provided wind speed and direction information to supplement that obtained from the sodar. Balloon flights were made every 20 to 30 min from about 1630 to about 2000–2100 PDT. After that, strong and gusty winds in the first 100 m above the surface prevented balloon flights.

Wind velocity components could be determined from the tower-mounted anemometers to an accuracy of approximately 0.05 m/s, and temperatures at the towers and on the balloon instrument package could be measured with an accuracy of ~0.2 K or better.

3. Ambient Meteorology

3.1. Synoptic meteorology

Measurements were taken on seven nights, beginning on the evening of 3 October, 1986 and extending through the morning of 10 October, 1986. Except for the first

night, the weather was quite favorable, with clear skies, generally weak winds aloft, and consistent down-valley winds forming after sunset. A high pressure center produced generally northerly or northwesterly winds at 700 hPa over the experimental area during the entire period. The Doppler sounder, however, showed that ridge-top winds during this period usually had a down-valley, or southerly, component, which probably arose from a mesoscale drainage flow from the Blue Mountains south of the observation site.

3.2. Valley Meteorology

3.2.1. *Evolution of Valley Temperature and Wind Structure*

Sequential Tethersonde® profiles taken from the valley center showed similar temperature and wind structure evolution from night to night. Analyses have emphasized the nights of 4, 5, and 8 October. On these nights the down-valley winds and the downslope winds on the sidewalls were particularly steady for most of the night. In this section, temperature and wind structure evolution during the evening transition period are illustrated by features from the night of 5 October.

In Figure 2, the first potential temperature sounding of the 5 October sequence, at 1546 PDT, found a well-mixed, nearly constant potential temperature atmosphere. At this time, the west sidewall had been in shadow for nearly $1\frac{1}{2}$ h. The constant potential temperature layer contained up-valley winds with speeds of 1

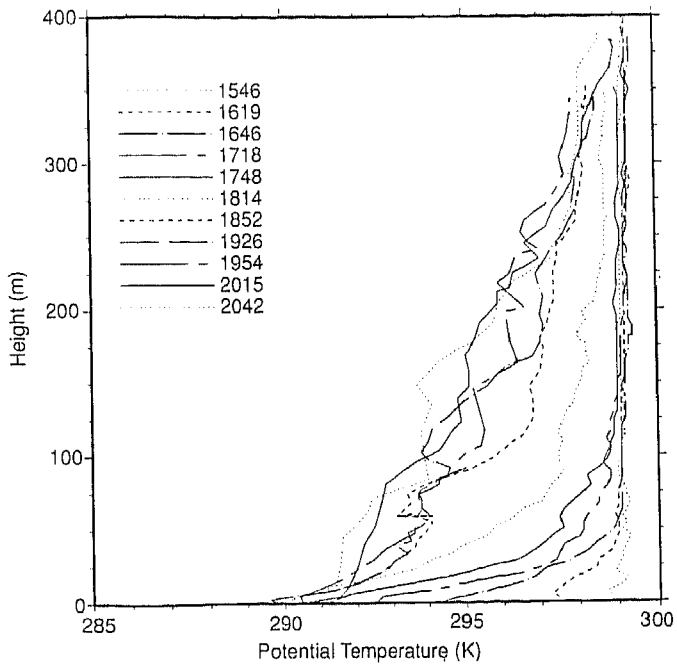

Fig. 2. Sequence of tethered balloon temperature profiles for 5 October. Sounding sites (PDT) are indicated in the legend. Initial profile (1546) is on the right and the final profile (2042) is on the left.

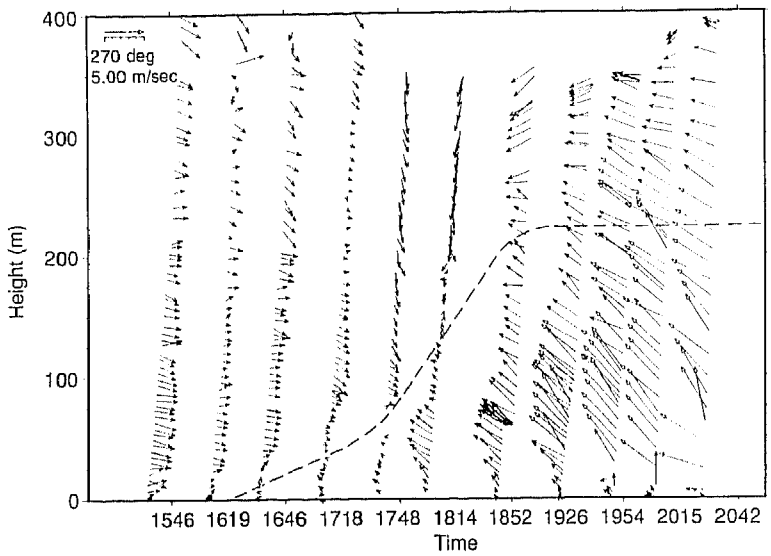

Fig. 3. Tethered balloon wind profiles for 5 October. The top of the down-valley flow region in the valley is indicated by the dahsed line.

to 3 m/s (Figure 3). Subsequent temperature soundings, taken at roughly 30-min intervals, showed rapid cooling in a growing stable boundary layer above the valley floor. The cooling was confined initially to this near-ground layer, with the inversion attaining strengths of 7 to 8 K through depths of less than 100 m. Winds within the growing inversion layer reversed to down-valley, whereas the winds in the upper levels of the valley maintained their up-valley direction. The character of the temperature structure evolution began to change between the 1748 and 1814 PDT soundings, and then changed more abruptly between the 1814 and the 1852 PDT soundings, when the east sidewall went completely into shadow and the winds in the upper part of the valley atmosphere reversed to down-valley and strengthened. This change was a typical feature of the meteorology of this valley during the exprimental period. Specifically, the initial shallow, but intense, near-ground temperature inversion became mixed through the entire valley depth so that the upper levels of the valley atmosphere began to cool at a faster rate than the surface layers. Eventually, over the next 1 to 2 h the mixing associated with the strengthening down-valley winds distributed the cooling through the valley atmosphere so that the temperature inversion became much less intense.

In the lower part of the valley atmosphere, unusual and distinctive temperature structure layers were found after the 1814 PDT sounding. Specifically, a nearly constant potential temperature layer developed and was capped by strong potential temperature jumps. An example can be seen in Figure 2 in the 2042 PDT sounding between 90 and 140 m. These temperature structure layers are quite similar in

form and behavior to the layers that developed during an evening transition period in Colorado's Eagle Valley, as described by Whiteman (1986). In the Eagle Valley case, these features were transitory, observed only during the evening transition period. The constant potential temperature layer was thought to be the layer into which downslope flows converged, resulting in a gradual ascent of the top of this layer (i.e., the ascent of the potential temperature jump). In the Eagle Valley, these layers evolved smoothly in time, but in the Touchet Valley the general evolution was less regular.

Unfortunately, because strong down-valley winds developed late in the evening. Tethersonde® ascents could not be continued through the night to investigate whether the temperature structure features were transitory. As well be discussed in Section 6, a decrease in the sidewall inversion depth with increasing downslope distance appears to be related to the presence of an adiabatic layer in the valley atmosphere, and such a decrease is normally found during most of the night. This suggests that constant potential temperature layers may, in fact, be present over much of the night. On 8 October, when a Tethersonde® sounding made just before sunrise did now show the distinctive temperature structure features of the previous evening, the downslope development of the slope-flow inversion depth during this period was not representative of the structure for most of the night. At this time the question of the persistence of adiabatic layers in the valley atmosphere remains unresolved.

The general features of inversion buildup differed little from night to night. For this analysis, the inversion top was estimated as the elevation where the slightly stable layer in the upper levels of the valley gave way to a more distinctly stable atmospheric structure below. Inversions began to form between 1530 and 1630 PDT depending, presumably, on day-to-day differences in valley energy budget, cloudiness, and above-valley wind regime. The data show that inversions grew to the full depth of the valley (225 m) in 2 to 3 h and that further growth was precluded.

Inversion strength (potential temperature difference between the top of the inversion and the surface) on 5 October behaved in a manner consistent with the temperature profile evolution and initially increased rapidly while a shallow layer became cooled over the valley floor. This occurred over roughly the first hour of cooling. The inversion strength then increased less rapidly while the shallow temperature deficit mixed through the valley depth. After another 2 or 3 h, the inversion strength reached 7 to 8 K.

Doppler sodar-measured winds were also fairly consistent from night to night. The wind analyses showed that down-valley winds began between 1800 and 1900 PDT and reversed to up-valley around 1000 PDT the following morning. Nocturnal winds were strongest (6 to 7 m/s) at about the 75-m level. Winds in the lower levels of the valley atmosphere tended to be aligned very well with the valley's longitudinal axis.

3.2.2. *Cross-Valley Temperature Structure*

The initial assumption about the cross-valley temperature structure was that, in the region above the katabatic layer on the sidewalls, the isotherms would be nearly horizontal. In that event, a measurement of the temperature at the top of a sidewall tower would provide a good measure of the ambient temperature, i.e., the temperature in the center of the valley, and the inversion strength measured at the sidewall tower would be nearly equivalent to the temperature difference between the sidewall and the ambient air.

The structure actually observed was considerably more complicated. On the east sidewall, at least, the local inversion seemed to be generally well contained by the sidewall towers, so that the temperature gradient near the top of the towers was usually small. However, comparisons of the temperatures at the tops of the towers with those recorded by the Tethersonde® at the same elevation consistently showed differences. At tower A, $T_{\text{teth}} - T_{\text{tower}}$ averaged 0.7 ± 0.9 K, while at towers B and C the differences were 0.3 ± 0.7 K and -0.1 ± 0.7 K, respectively. The large standard deviations are misleading. When $T_{\text{teth}} - T_{\text{tower}}$ was plotted individually for each night, there were systematic trends with time that repeated from night to night. Specifically, the temperature differences at towers A and B tended to increase while the evening progressed. This trend, however, was not obvious at tower C. Figure 4 shows an example for the data from tower A. Because we could not collect tethered balloon data later in the evening, it is not known whether this behavior persisted throughout the night.

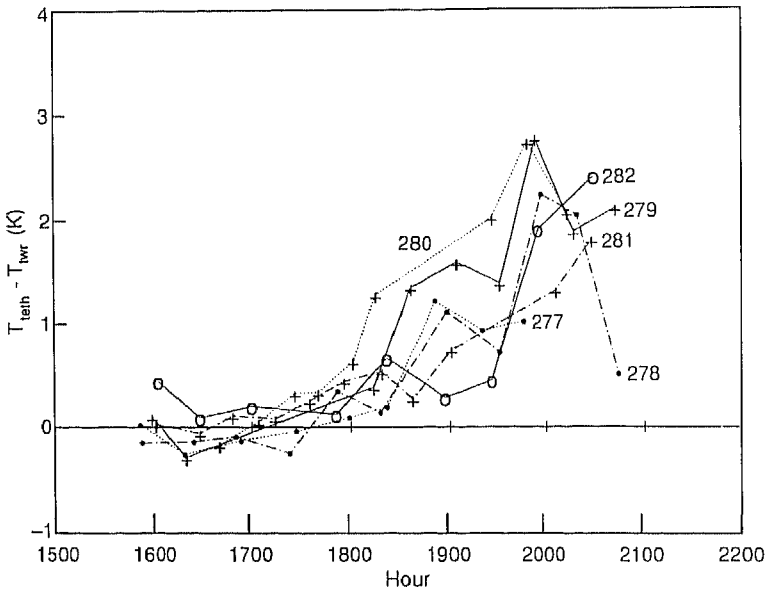

Fig. 4. Temperature difference between top of tower A (T_{twr}) and the center of the valley at the corresponding elevation (T_{teth}) for nights of 4 October (277) through 9 October (282).

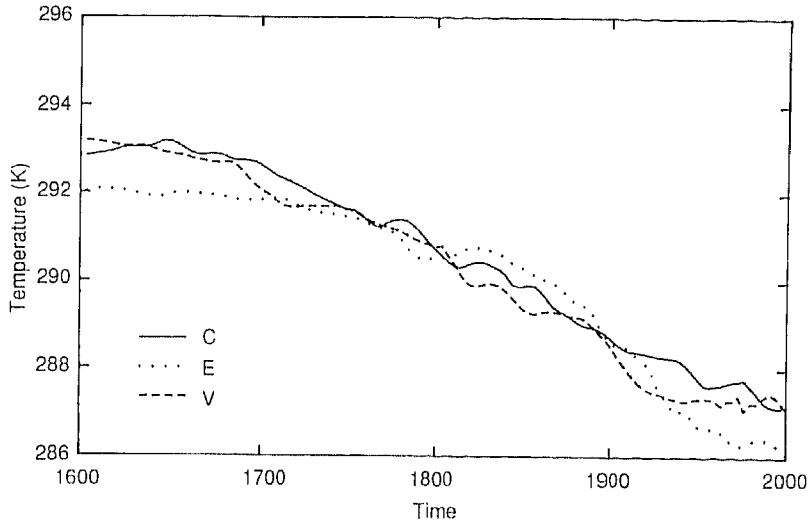

Fig. 5. Temperatures at the tops of Towers C, E, and of the 61-m tower in the center of the valley (V) on 8 October.

A further illlustration of the presence of cross-valley temperature gradients is shown in Figure 5. This figure shows temperature time series measured at the tops of towers C and E, on opposite sides of the valley, and at the main tower V in the center of the valley. The tops of all three towers were at approximately the same elevation above the valley floor. The figure covers a 4-h period for 8 October. The horizontal temperature differences between the valley center and the sidewalls were often on the order of 1 K and lie well outside the range of precision and accuracy that we attributed to our instruments. The gradients shown are highly variable but significant, and, as will be shown, cause problems in the interpretation and analysis of our data.

4. Characteristic Parameters of Slope Flows

Figure 6 shows wind and temperature profiles at tower B for a 10-min period on the morning of 5 October. The inversion and the local maximum in the downslope wind speed indicate the presence of katabatic slope flows. These flows persisted for most of the night and were found on all nights of our experimental period. However, the relative magnitudes of the downslope winds and the strengths and depths of the inversions varied with time and tower location, and some means of characterizing these variations is needed.

Descriptions of katabatic flows over simple slopes have made use of a variety of parameters that succinctly summarize some of their principal features. These include scale height, scale velocity, buoyancy or temperature deficit, inversion

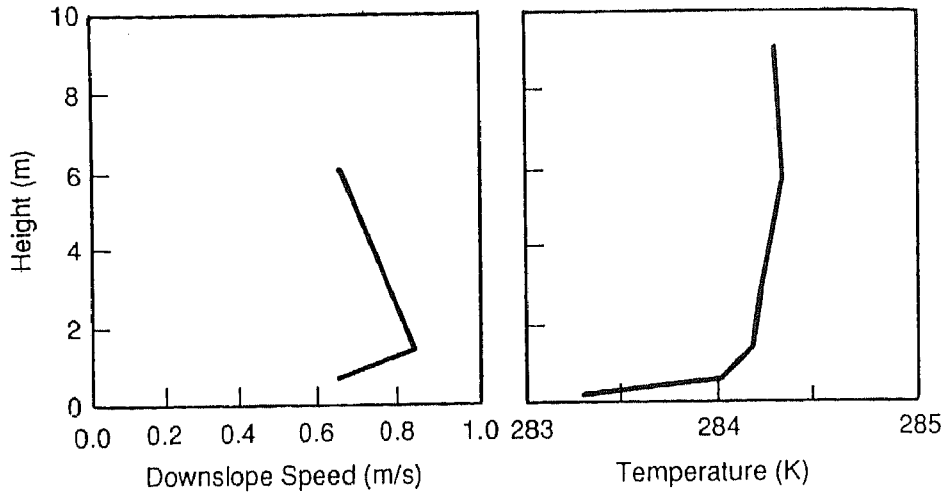

Fig. 6. Wind and temperature profiles at tower B from 0100 to 0110 PDT on the morning of 5 October.

depth, and height of the wind speed maximum. Similarly, in flows down valley sidewalls, it would be useful to characterize the depth, strength, and structure of the local inversion and the downslope wind profile in terms of a few parameters.

By assuming a constant eddy diffusivity, Prandtl (1942) derived analytic expressions for the slope wind and temperature profiles. Filliger *et al.* (1987) found these profiles useful in fitting their wind and temperature data collected near the bottom of a long slope (965 m below the the summit) in Switzerland. However, the Prandtl profile gave a poor representation of the shape of our observed temperature profiles near the tops of the sidewall towers. The fit to the velocity profiles was also poor, although ambient cross-valley winds may have been partly responsible for this.

We had considerably better success in fitting the east sidewall temperature profiles with an expression of the form

$$T(n) = T(9\,m) - \Delta T * \exp(-n/h)\,, \tag{1}$$

where ΔT is the magnitude of the inversion strength and h is a measure of the inversion depth. (In the discussions to follow, we shall refer to ΔT and h as the inversion strength and inversion depth, respectively, although h is more properly an e-folding length rather than an inversion depth.) An example of this fit is shown in Figure 7, where data obtained at tower A on the night of 5–6 October are plotted.

The inversion was generally contained within the 9-m height of the towers on the east sidewall, but not on the west. Even so, the exponential parameters are useful in providing an approximate description of the temperature profiles.

Attempts to find a similarly useful set of parameters to describe the wind profiles

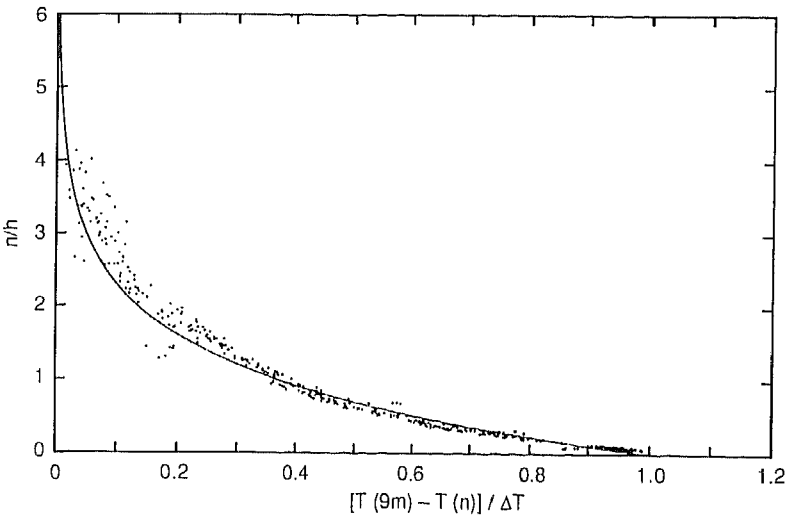

Fig. 7. Scatter plot of temperature differences on Tower A, normalized by the inversion strength ΔT, as a function of n/h. The line is Equation (1).

were much less sucessful. There were three principal problems. The first was that three levels of wind measurements on each of the sidewall towers were not sufficient to resolve the shapes of the wind profiles. Although there was generally clear evidence of a low-level maximum in the downslope wind component during significant portions of the evening and night, its exact height and magnitude could not be determined. Second, model simulations suggest that the highest measurement level (~ 6 m) was not high enough to lie above the katabatically driven layer. Finally, whereas the wind measured at the center of the valley frequently showed a negligible cross-valley component, this was not always the case. Moreover, it is not obvious that the ambient winds at the valley center were the same as at the valley sidewalls. This ambiguity in the contribution (katabatic or ambient) to the downslope wind component and the lack of vertical resolution in the measurements made it impossible to assign a meaningful magnitude or depth scale to the sidewall wind data.

5. Dependence of Slope Flow Parameters on Time and Valley Meteorology

5.1. Time relationships

Understanding the propagation of shadows through the valley during the evening transition period is useful for interpreting the meteorological data. Sunset times for towers E and F were estimated from the time when net radiation dropped suddenly. A close relationship is expected between the sign reversal of net radiation and the initiation of solar shading on the west sidewall because the sun is high in the sky when shading abruptly occurs. This was not true for the east

sidewall, and local sunset times for towers A, B, and C were determined visually by an observer on the valley floor. Local sunset times of 7 October for towers A, B, C, E, and F were 1802, 1740, 1710, 1416, and 1531 PDT, respectively.

Astronomical sunset, i.e., sunset on a hypothetical unobstructed horizontal surface at the latitude and longitude of the field site, was 1822 PDT on 7 October. Thus, local sunset on the west sidewall is much earlier than astronomical sunset, but local sunset at the uppermost tower on the east sidewall occurs only 20 min in advance of astronomical sunset. At site E, local sunset occurs $3\frac{3}{4}$ h before that at site A. The sign reversal of net radiation, the buildup of a temperature inversion over the slope, and the development of downslope flow occur much earlier on the west sidewall than on the east sidewall. Observations on the valley floor show that the valley temperature inversion begins to build at about 1600 PDT, nearly $1\frac{3}{4}$ h after sunset at site E, before any of the east sidewall sites are shaded, and before the daytime up-valley flows are reversed. Reversal of the daytime up-valley winds through the entire valley depth occurs at about 1830 PDT.

5.2. Sidewall inversion strength

At the east sidewall, night can be conveniently divided into two portions, a transition period in the first hour or so after local sunset and an approximately steady-state period that persists throughout the remainder of the night until sunrise the next morning. The sidewall inversion strengths generally reached their maximum values during the transition period, and then decreased to roughly constant values for the remainder of the night, although there were occasional periods in the early morning hours when the inversion strength might increase temporarily. At tower A the range of maximum strengths were between about 2.5 and 5 K, at tower B between about 2 and 4.5 K, and at tower C between about 1.5 and 2.5 K. For the remainder of the night after the evening transition, the inversion strengths at towers A and B were generally quite similar (~ 1.2 K) and about 50% greater than at tower C (~ 0.8 K). Figure 8 gives an example of the time evolution of the sidewall inversion strengths for 8–9 October.

The valley wind speed was a significant factor in determining slope flow characteristics. Figure 9a shows a scatter plot of the inversion strength at tower A as a function of the along-valley wind speed near the valley center at the elevation of tower A, as determined from the sodar measurements, for all six nights of the experimental period. Also shown are means and standard deviations of the inversion strengths for each 1-m/s speed interval. Although there is considerable scatter in the data, particularly at the lower wind speeds, the trend of decreasing inversion strength with increasing wind speed is clear. The lower speeds were usually found during the evening transition periods; after this time, the wind speeds in the valley increased and the inversion strength on the sidewall decreased. There is only one instance of an inversion as strong as 2 K when the along-valley wind speed was 4 m/s or higher. It appears that a low valley wind speed is a necessary condition for a strong sidewall inversion to form. A low valley wind speed is not a sufficient

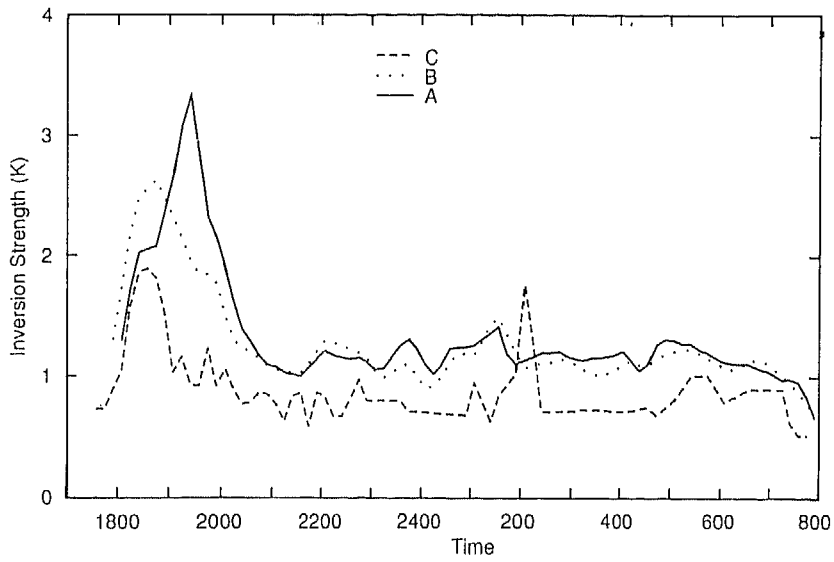

Fig. 8. Inversion strengths at Towers A, B, and C on the night of 8–9 October.

condition, however, as can be seen from the wide range of inversion strengths found for speeds less than 4 m/s.

The behavior at tower B was quite similar to that at tower A, but at tower C there were some significant differences (Figure 9b). As noted above, the largest inversion strengths during the transition period are much smaller at tower C than at towers A and B, and the steady-state strengths are weaker as well. Figure 9b also shows a relative scarcity of data for low wind speeds. This arises primarily because the down-valley winds developed relatively quickly at the lower elevations, so that by the time an inversion began to form at tower C, the ambient winds at that level were already well established.

Thus, there seem to be two features that contribute to the weaker inversions at tower C. First, the ambient winds at this level tend to be higher than at the levels of towers A and B because of the low-level jet in the down-valley wind component. This results in greater turbulent mixing, thereby reducing the strength of the inversion. However, even for similar ambient wind speeds, the inversion strengths are weaker, as can be seen by comparing Figures 9a and 9b. A possible explanation for this has been given by Manins and Sawford (1979), who developed a layer-integrated model for drainage winds over simple slopes. Their model predictions depend upon their entrainment assumptions and must, therefore, be treated with some caution. In any event, their model showed that the inversion strength decreases with increasing slope distance from the crest of the hill. They argued that cooled air moving down the slope encounters denser ambient air and a larger fraction of the cooling is required to maintain the buoyancy deficit in the cooled layer. This appears consistent with the observations made at Dayton;

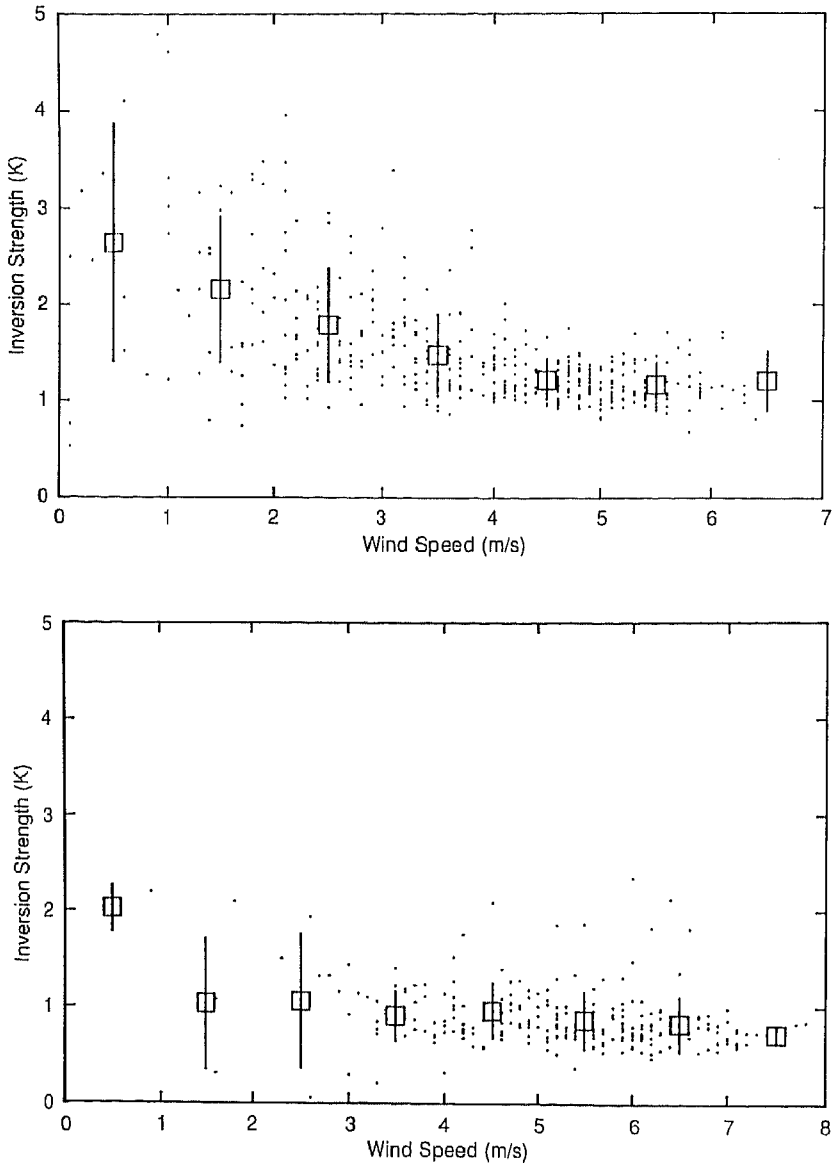

Fig. 9. (a) Scatter plot of ΔT at Tower A versus down-valley wind speed at the elevation of tower A. (b) Scatter plot of ΔT at Tower C versus down-valley wind speed at the elevation of tower C. Boxes: means; lines: standard deviations.

however, on Rattlesnake Mountain, there was no consistent trend with downslope distance in the behavior of the inversion strength (Horst and Doran, 1986). The reason for this difference may be related to the much stronger stratifications found in the Dayton valley compared to those at Rattlesnake Mountain. The predicted decrease of inversion strength with downslope distance is accentuated by stronger

ambient stabilities. Any tendency for ΔT to decrease with increases in ambient stability would thus be more evident at the Dayton site.

5.3. Sidewall inversion depth

During the evening transition period, the inversion depths (i.e., the e-folding depth defined earlier) at all three towers increased so that their maximum values occurred around 2030 PDT. Typical maximum depths were about 3 m at tower A and 2 m at towers B and C. After this initial period, the depths decreased slowly to about 2 m at tower A and 1 m at towers B and C. The behavior at towers B and C was generally similar except that tower C often showed an increase in h to about 1.7 m for a few hours before sunrise. Figure 10 shows an example of the time evolution of sidewall inversion depths for the night of 4–5 October. This dependence of the inversion depth on downslope distance is in marked contrast with that found over simple slopes.

Manins and Sawford (1979) and Nappo and Rao (1987) used models to calculate the behavior of h', the momentum depth for katabatic flows. This depth scale is related to the height to which the katabatic winds extend, and for negligible ambient winds is defined by the set of equations

$$Uh' = \int_0^\infty u \, dn' \tag{2}$$

and

$$U^2h' = \int_0^\infty u^2 \, dn'. \tag{3}$$

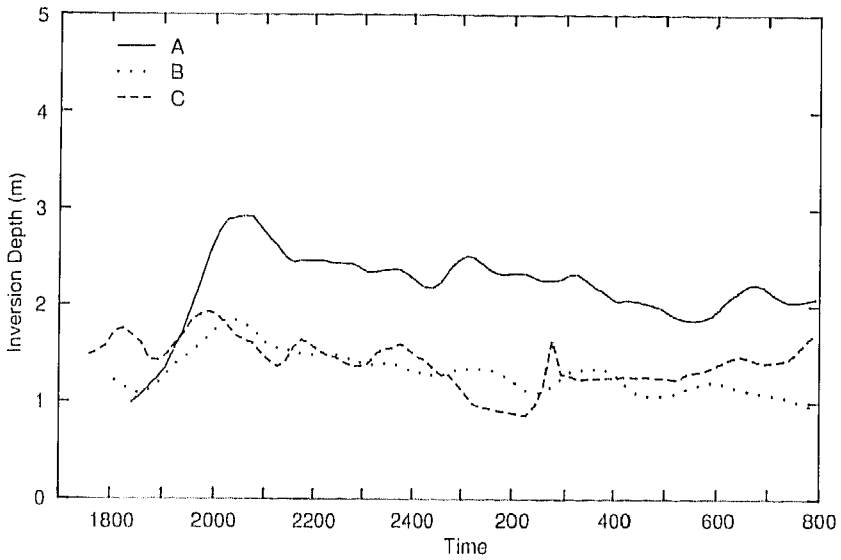

Fig. 10. Time evolution of the inversion depths for the night of 4–5 October.

In the presence of downslope ambient winds the momentum depth is difficult to define or measure. Even if there had been no ambient winds, numerical simulations suggest that our wind measurements did not extend far enough above the slope to lie above the katabatic flows, so that a determination of the momentum depth would not have been possible. However, Horst and Doran (1986) showed that in the Manins and Sawford model the momentum depth and the inversion depth are proportional, a conclusion that is supported by observations over simple slopes. The Manins and Sawford model predicted that the momentum and inversion depths should increase faster with downslope distance as the stable stratification of the ambient atmosphere increases.

Whereas Manins and Sawford used a constant buoyancy flux as their lower boundary condition, Nappo and Rao decreased the surface temperature uniformly in time until a specified ground temperature deficit was achieved and held the heat flux constant from then on. Nappo and Rao also claim that Manins and Sawford's assumption of an entrainment rate independent of stratification is not justified, and reach a different conclusion about the growth of h'. From their calculations, they conclude that the rate of increase of h' with downslope distance decreases as the ambient stratification is increased; this dependence on stratification is just the opposite of the Manins and Sawford conclusion.

Neither model deals with ambient stratification changing with elevation, which occurs in valleys, and in such circumstances it is not obvious that the momentum and inversion depths should behave similarly. This issue is discussed further in the section describing the results of our numerical simulations.

The area found by integrating under the temperature inversion profile is proportional to the total buoyancy force driving the katabatic slope flow; this force may be defined as the integrated buoyancy deficit. For the exponential temperature profile, this area is equal to the product of the inversion strength ΔT and the inversion depth scale h. The product $h * \Delta T$ decreases with downslope distance, from a typical value of 2.5 m-K at tower A to 1.5 m-K at tower B and 1 m-K at tower C. In contrast, on Rattlesnake Mountain the integrated buoyancy deficit increased monotonically with downslope distance, in keeping with the predictions of the model of Manins and Sawford.

The observed behavior of the temperature structure is summarized in Table II. The first column lists the predictions of the Manins and Sawford model for the behavior of three quantities: the inversion depth (actually, the momentum depth, which is proportional to the inversion depth in their model), the inversion strength, and the integrated buoyancy deficit. The second column, labeled as "Simple Slope", lists the observed behavior on Rattlesnake Mountain at three towers, A, B, and C, placed in the same relative order (top to bottom) as at Dayton. The third column refers to the observations on the valley sidewall at Dayton. The notation A > B for inversion depth, for example, means that the inversion depth at tower A is greater than that at tower B.

TABLE II

Relative values of inversion depths, inversion strengths, and integrated buoyancy deficits from model predictions for a simple slope, measurements on a simple slope, and measurements on a valley sidewall

	Manins and Sawford model prediction	Simple slope	Valley sidewall
Inversion depth	A < B < C	A < B < C	A > C ~ C
Inversion strength	A > B > C	A ~ B ~ C	A ~ B > C
Integrated buoyancy deficit	A < B < C	A < B < C	A > B > C

5.4. Downslope winds

Wind measurements were made at nominal heights of 0.7 and 1.5 m at all three towers on the east sidewall, with a third measurement at 3.5 m on tower A and ~6 m at towers B and C. The wind at the 1.5-m level often had the largest downslope component, so that even though there is not sufficient resolution in our wind measurements to identify the height of a downslope jet, it is reasonable to look at the 1.5-m level winds as a rough indicator of the strength of the katabatic flow. In the discussion to follow, unless specified otherwise, references to a downslope wind are to be understood as the downslope component at ~1.5-m height at each tower.

At tower B, the downslope wind had typical values in the range of 0.6 to 0.8 m/s for most of the nights. At tower A the downslope wind was generally a few tenths of a meter per second lower; at tower C the downslope wind had magnitudes comparable with those at A and B but was much more variable.

Because the quantity $h * \Delta T$ is proportional to the total buoyancy force driving the katabatic flow, a correlation between that quantity and the strength of the katabatic flow was expected. This expectation was realized, but only when the down-valley winds were relatively weak. For along-valley winds less than 2 m/s, there was a tendency for the downslope winds to increase with $h * \Delta T$, but this tendency disappeared for stronger along-valley winds. This shows that once the valley wind systems are well established, fluctuations in the sidewall integrated buoyancy deficit have little effect on the downslope wind component. It is possible that the downslope wind maximum, its height, or the total downslope volume flux may depend on the integrated buoyancy deficit, but these possibilities could not be tested with only three anemometers at each of the sidewall towers.

Although the inversion was usually contained by the vertical extent of the temperature sensors on the towers on the east sidewall, model results suggest that a complete measurement of the katabatic wind profile would require additional instruments at higher levels to determine their vertical extent and additional instruments at low levels to resolve the local katabatic wind maximum.

6. Numerical Model

6.1. Model description

A two-dimensional slope-flow model was used to provide additional insight into the structure of slope flows in simple valleys. Our observations were used to describe the ambient environment that provided the boundary conditions for the model. The model was then used to perform a series of numerical experiments to examine the mechanisms responsible for the observed features of the slope flows.

The model assumes that the slope angle is constant, and the equations to be solved are written in a coordinate system that is parallel (s component) and normal (n component) to the sloping surface. Prognostic equations are solved for the downslope wind component u, the cross-slope component v, the turbulent kinetic energy e, and the potential temperature difference θ'. Here, θ' is the difference between the potential temperature in a layer affected by the cooling of the sidewall surface and the ambient potential temperature found at the same elevation in the middle of the valley.

The equation for the downslope wind component u is

$$\frac{\partial u}{\partial t} = -u\frac{\partial u}{\partial s} - w\frac{\partial u}{\partial n} - g\frac{\theta'}{\theta_0}\sin\beta + \frac{\partial}{\partial n}\left(K_m\frac{\partial u}{\partial n}\right) + \frac{g}{\theta_0}\cos\beta\frac{\partial}{\partial s}\left(\int_n^{h_r}\theta'\,\mathrm{d}n\right), \tag{4}$$

where w is the wind component normal to the slope, β is the slope angle, K_m is a turbulent exchange coefficient for momentum, θ_0 is the ambient potential temperature, and h_r is the height where θ becomes zero. This equation is the same as that used by Nappo and Rao (1987) in their model.

The continuity and thermodynamic equations are given by

$$\frac{\partial u}{\partial s} + \frac{\partial w}{\partial n} = 0 \tag{5}$$

and

$$\frac{\partial \theta}{\partial t} = -u\frac{\partial \theta}{\partial s} - w\frac{\partial \theta}{\partial n} + \frac{\partial}{\partial n}\left(K_h\frac{\partial \theta}{\partial n}\right), \tag{6}$$

where K_h is a turbulent exchange coefficient for heat.

The turbulent kinetic energy (TKE) e is computed from

$$\frac{\partial e}{\partial t} = -u\frac{\partial e}{\partial s} - w\frac{\partial e}{\partial n} + K_m\left\{\left(\frac{\partial u}{\partial n}\right)^2 + \left(\frac{\partial v}{\partial n}\right)^2\right\} + \frac{\partial}{\partial n}\left(K_e\frac{\partial e}{\partial n}\right) - \frac{g}{\theta}K_h\frac{\partial \theta}{\partial n}\cos\beta[F] - \frac{c_\epsilon(2e)^{3/2}}{l}, \tag{7}$$

where the usual buoyancy production term is modified by a factor F. This factor arises from the effects of the slope-parallel heat flux (Horst and Doran, 1988) and is a function of the local shear and the ratio of the horizontal to normal heat fluxes. For our simulations, F usually did not differ significantly from a value of 1. In Equation (7), K_e is an exchange coefficient for TKE, c_ϵ is a constant equal to 0.0556 (Brost and Wyngaard, 1978, 1979), and l is a mixing length given by

$$\frac{1}{l} = \frac{1}{kn} + \frac{1}{l_0}. \tag{8}$$

The coefficient k is von Kármán's constant and l_0 is a limiting mixing length given by

$$l_0 = 0.10 \frac{\int_0^\infty qn \, dn}{\int_0^\infty q \, dn}, \tag{9}$$

where q^2 is twice the TKE (Mellor and Yamada, 1982).

The turbulent exchange coefficients K are calculated from the turbulent kinetic energy through the equation

$$K = Cla(e)^{1/2}, \tag{10}$$

where l is a mixing length, and the coefficient a has the value 0.540. The constant C has values of 1.0, 1.15, and 0.5 for momentum, heat, and TKE, respectively. These values for C represent a simplification of a slightly more complex scheme developed by Mellor and Yamada (1982) in which C depends on the flux Richardson number. For the range of stabilities found in our simulations, the model results were found to be rather insensitive to variations in the values of C used.

The equation for the TKE also contains the cross-slope (down-valley) wind component v, which is calculated from

$$\frac{\partial v}{\partial t} = \frac{\partial}{\partial n}\left(K_m \frac{\partial v}{\partial n}\right). \tag{11}$$

Cross-slope winds at the top of the model domain were assumed equal to the observed along-valley winds in the center of the valley at the corresponding heights. The vertical distribution of v in the model domain was then found from the above equation.

The model domain contained 13 points in the slope parallel direction and 15 in the normal direction. A staggered grid was used in which θ, e, and w were offset from the u and v velocity components by half a grid increment in the horizontal. The slope parallel spacing was 50 m. The normal spacing for the (e, w) grid points varied from 0.30 m near the surface to 40 m at the top of the domain (100 m). The quantities u, v and θ were defined at points midway between the (e, w) grid points.

One external grid point was defined at the top of the model, and e was set equal to a background value of 10^{-4} m^2/s^2 there. In Equation (9), this marked the actual upper limit of integration in the calculation of l_0.

The lower boundary condition for the thermodynamic equation describing the behavior of θ' was obtained by specifying the temperature of the air at the surface. These near-surface temperatures were estimated from extrapolations of sidewall tower temperature profiles to the surface, and do not, strictly speaking, correspond to the radiating temperature of the soil. However, for simplicity, the term "surface temperatures" will be used for this quantity.

During the course of our observations, both the ambient valley temperature structure and the local sidewall surface temperatures changed. During a simulation, these changes were approximated by linear interpolations in time between their initial and final values. The final steady-state model results depended primarily on the ambient temperature and wind fields at the end of the simulation, and showed little dependence on the initial temperature or the rate of cooling.

At the upstream boundary (the ridge line), only the ambient temperature was allowed to change; values of u, v, etc., were assumed fixed at their initial values. The downstream boundary (near the valley floor) used a zero-gradient condition in the downslope direction for all quantities. At the top of the model, u and v were set equal to ambient values near the center of the valley. In general it was assumed that there were no cross-valley ambient winds. Sodar measurements showed that this was not always true but it was often a good approximation and greatly simplified the construction of the model.

In a typical simulation, the initial temperature and the down-valley wind profiles were specified. The model was run for an initial period, normally 2 h, during which the temperature profile was held fixed but other variables were allowed to come to equilibrium. At the end of this 2-h period, cooling of the surface began and the ambient temperature began to change as well. The model time step was 0.5 s.

6.2. Model simulations

Three sets of numerical simulations were carried out. The first set utilized fairly simple temperature profiles to examine the basic response of the modeled slope flows to ambient stratification. This also allowed us to compare our model results with the results obtained by previous investigators. The second set of simulations used measured temperature profiles from the Dayton experiments in an effort to reproduce the observed behavior of the slope flows on selected nights. Finally, a series of sensitivity tests were carried out to isolate those features of the ambient conditions that were most important in determining the slope flow characteristics, and to gain additional insight into the structure of slope flows. These three sets of simulations are described below.

The first set of simulations used ambient temperature profiles with constant stratification. The ambient down-valley wind component v was specified as a jet with a peak value of 5.4 m/s at a height of approximately 90 m above the valley

floor. Following the initial cooling procedure of Nappo and Rao, a constant temperature difference between the sidewall surface and the ambient atmosphere at the same elevation above the valley floor was specified. Momentum depths, h', were calculated using Equations (2) and (3). The temperature profiles that resulted from these simulations were then fit to the exponential curve described by Equation (1), and values of h and ΔT were computed from a least-squares fit to the temperature profiles over the first 9 meters above the slope, as had been done with the actual data. The dependence of h on downslope distance was then compared with predictions from the model of Nappo and Rao (1987).

For an adiabatic ambient lapse rate, h' and h were found to increase monotonically with downslope distance, but when the stability was increased, h and h' increased at a slower rate. These results for h' and h are qualitatively similar to those reported by Nappo and Rao for h'.

Additional tests were run in which the ambient stratification was allowed to change abruptly with height, as was seen in many of the temperature soundings discussed earlier (e.g., Figure 2). It was found that in descending along the sidewall from a region of strong ambient stratification into an adiabatic layer, the inversion depth h would decrease and then begin to increase again because of the distortion of the temperature profiles in the transition region. This behavior illustrates the sensitivity of this scaling parameter to the details of the ambient temperature environment in which the katabatic flows develop. In contrast, the momentum depth h' increased more rapidly when the adiabatic layer was entered, as would be expected. Thus, when the stratification changes with height, the two depth scales, h and h', no longer evolve similarly with downslope distance. This is a marked difference from the behavior over simple slopes with constant ambient stratification.

The second set of simulations tested the model's ability to simulate the observed slope flow characteristics. The evenings of 4, 5, and 8 October were chosen as test periods. The data from the final Tethersonde® soundings on those nights were used to construct final ambient temperature and wind profiles for the model. An adiabatic initial state was assumed. Final surface temperatures were estimated from extrapolations of the observed temperature profiles on towers A, B, and C.

The assignment of the final ambient temperature profiles was difficult because the Tethersonde® soundings showed significant spatial and temporal irregularities. The possible existence of any cross-valley temperature gradients further complicates the problem of choosing the proper ambient state for the model, as will be shown in the examples below. In practice, piecewise linear approximations for the ambient temperature and down-valley velocity profiles were used.

The results of this second set of simulations are summarized in Table III. The inversion depths at tower A are about 20 to 30% lower than the observations for all three simulations. The depths at the other two towers generally show better agreement with observations, as do the relative ordering from towers B to C. For 4 October, the simulated inversion strengths at all three towers agree with the

TABLE III

Comparisons of the observed and calculated values of inversion depth h, inversion strength ΔT, and their product for 4, 5, and 8 October

	Tower	Observed			Simulated		
		h (m)	ΔT (K)	$h^*\Delta T$ (m-K)	h (m)	ΔT (K)	$h^*\Delta T$ (m-K)
4 October	A	2.3	1.3	3.0	1.6	1.3	2.1
	B	1.5	1.4	2.1	1.6	1.4	2.2
	C	2.1	0.9	1.9	1.9	0.9	1.7
5 October	A	2.7	1.4	3.8	1.9	2.1	4.0
	B	2.2	1.0	2.2	1.5	2.0	3.0
	C	2.1	0.9	1.0	1.8	1.2	2.2
8 October	A	1.6	2.1	3.2	1.3	2.6	3.4
	B	1.2	1.5	1.8	1.5	2.0	3.0
	C	1.8	0.9	1.6	1.8	0.6	1.1

observations. For 5 and 8 October, the simulated inversion strengths are too large but the relative ordering of ΔT from tower to tower is reproduced properly. The product $h * \Delta T$ decreases with increasing downslope distance for all three cases shown in Table III. The model also shows $h * \Delta T$ decreasing, except for tower A on 4 October, where the low value of inversion depth makes the simulated integrated buoyancy deficit at tower A slightly less than that at tower B.

The poorer performance of the model in simulating the inversion strengths on 5 and 8 October can be attributed to the difficulty of establishing the proper ambient temperature profiles to use on these days. As noted earlier, Tethersonde® measurements often showed significant spatial variations during a sounding and from one sounding to the next; these fluctuations were particularly severe on the evening of 5 October. The temperature gradients between the center of the valley and the sidewalls were also significantly larger for the nights of 5 and 8 October than for the night of 4 October. Such differences are consistent with the calculated inversion strengths being too high for the later dates. Furthermore, they demonstrate clearly why measurements of the conditions in the center of the valley may not be sufficient to determine the nature of the slope flows.

Another difficulty is that measurements to determine the surface air temperatures were unavailable except at the three tower sites. Extrapolation to grid points outside the positions of towers A and C, which are located approximately at grid positions 5 and 10.5, respectively, are essentially educated guesses. This problem is compounded at the downslope end of the model because there is an increase in the actual slope angle below tower C whereas the model assumes a constant slope angle.

Despite these problems, the model captures many of the essential features of the slope flows on the valley sidewalls. As a result, it was used in a third set of simulations to examine some of the mechanisms responsible for the observed

features. The model was also used to give additional information about the structure of slope flows that was not measured.

Simulations were performed using different combinations of ambient stabilities, surface temperatures, and down-valley winds. For all of these simulations, a fixed potential temperature increment between the bottom of the valley and a point slightly above the ridge line was assumed. The profile of the ambient down-valley wind component v used in the first set of simulations was normally used in this set as well. A series of final ambient temperature profiles was then tested to see which ones yielded a behavior for h and ΔT that corresponded to our observations. For the first test, a set of surface temperature values was chosen, and a constant stability was defined between the surface and the ridge line (Profile 1 in Figure 11). This gave a monotonic increase in h from tower A to C (Test 1 in Table IV). However, if regions in which the potential temperature was constant with height were included (Profile 2 in Figure 11), as found in many of the Tethersonde® soundings in the later parts of the evenings, the simulations corresponded much more closely to observations (Test 2 in Table IV).

We found that a second condition was also required for good agreement between simulations and observations, viz., the surface temperatures must be chosen to yield the proper temperature differences between the ground and the ambient atmosphere. The "proper" choice was based on observations. If either the temperature differences were poorly chosen or the ambient potential temperature lacked a region of constant potential temperature, then the simulations failed to produce good agreement with observations. For example, Profile 3 in Figure 11

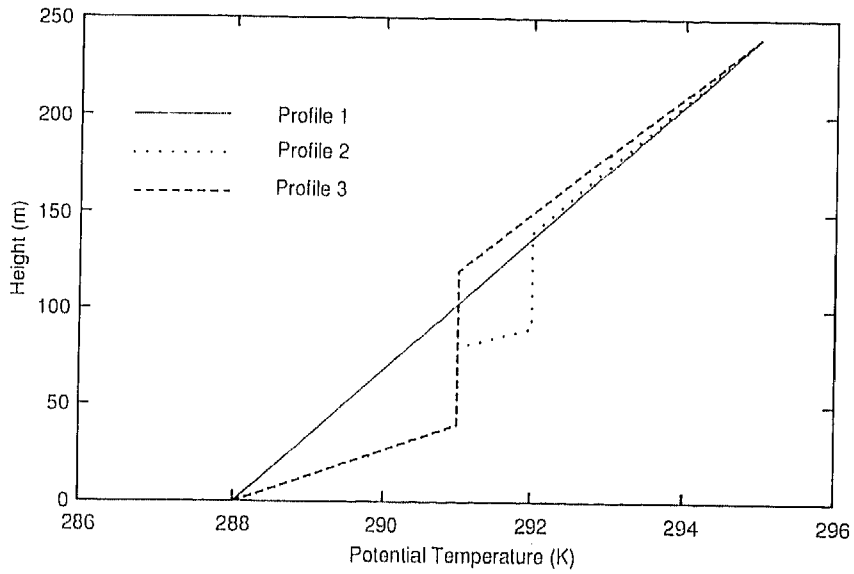

Fig. 11. Potential temperature profiles used for the simulations of slope flows in Table IV.

TABLE IV

Results of numerical simulations for various combinations of ambient temperature profiles, surface temperatures, and down-valley wind profiles

Test	h_A (m)	h_B (m)	h_C (m)	ΔT_A (K)	ΔT_B (k)	ΔT_C (K)
1	1.6	2.1	3.6	1.6	0.8	0.4
2	1.8	1.2	1.2	1.6	1.5	1.1
3	1.2	0.9	0.8	1.7	1.6	1.1

Test 1: Profile 1, Figure 11.
Test 2: Profile 2, Figure 11.
Test 3: As in Test 2, but with reduced ambient down-valley winds.

also yielded good results when the ground-ambient temperature differences were the same as those in Test 2, but poor results when they were not the same.

We remarked earlier that the behavior of the slope flows on the morning of 8 October was atypical. The valley potential temperature profile on that morning had no region of constant potential temperature, and the inversion depth measured at tower C was larger than at tower A or B. This feature was found on several mornings in the hours shortly before sunrise. Such behavior is consistent with the results of our test simulations, which show that decreases in h with downslope distance seem to require the existence of some adiabatic layer in the ambient atmosphere.

The down-valley wind was also expected to have a significant influence on the slope flow characteristics, but the effects are more difficult to test with the model. It was noted earlier that once the down-valley winds increase, the local inversion strengths on the sidewall drop below their maximum values attained during the transition period. This effect was attributed to enhanced vertical mixing on the sidewalls. The model cannot properly simulate this physical mechanism without using a surface energy budget that accurately determines the temperatures or the sensible heat fluxes at the lower boundary. The ambient down-valley wind in the model can be reduced, but if the surface temperatures are not affected, the inversion strength is unlikely to change significantly. This is shown in Test 3 in Table IV. For this test, the ambient winds were reduced to 25% of the values used in the earlier tests. This results in reduced values of h because the mechanically generated TKE is less and vertical mixing is suppressed.

The simulations also revealed information on some features of the slope flows that was not available from our measurements. Sensible heat fluxes at the surface were calculated from wind and temperature profiles using similarity theory. These results showed that the heat flux was not constant down the slope, varying irregularly by a factor of three between towers A and C, and decreasing to very small values below tower C. This decrease may be related to the previously discussed problems with the boundary conditions at the downslope edge of the model, but we are unable to test this. Observations also show that the use of a temperature

difference between the surface and the ambient air that is independent of downslope distance, as used in our first series of tests described previously, is also unrealistic for the Touchet Valley. A terrain-following three-dimensional model with a rather complete surface energy budget would be useful for determining the proper lower boundary condition for temperature.

Another feature of slope flows shown by the model is that their behavior is not as regular as one might conclude from simply examining the results listed in Table III. For example, in Test 2 described above, h is equal to 1.2 m at towers B and C, but is greater than 3 m just below tower B. This region in the model was characterized by a very sharp increase in the ambient potential temperature between 80 and 90 m above the valley floor (Profile 2 in Figure 11). When a different profile was used, without this region of sharp increase in potential temperature (Profile 3 in Figure 11), the large jump in the value of h disappeared. This behavior again shows the sensitivity of the model to the details of the ambient temperature field. If the actual slope flows are similarly sensitive, then variations from the behavior summarized in the last column of Table II should not be uncommon. An example is given in Figure 12, which shows the variation of h at towers A, B, and C on the night of 5–6 October. For most of the night the behavior is similar to that previously shown in Figure 10 for 4–5 October. However, there is a period of several hours before sunrise when the usual pattern is disrupted.

Finally, Figure 13 shows plots of the simulated wind and temperature fields at the positions of towers A, B, and C for the conditions used in Test 2. There is a slight strengthening of the katabatic winds between A and B, with a subsequent

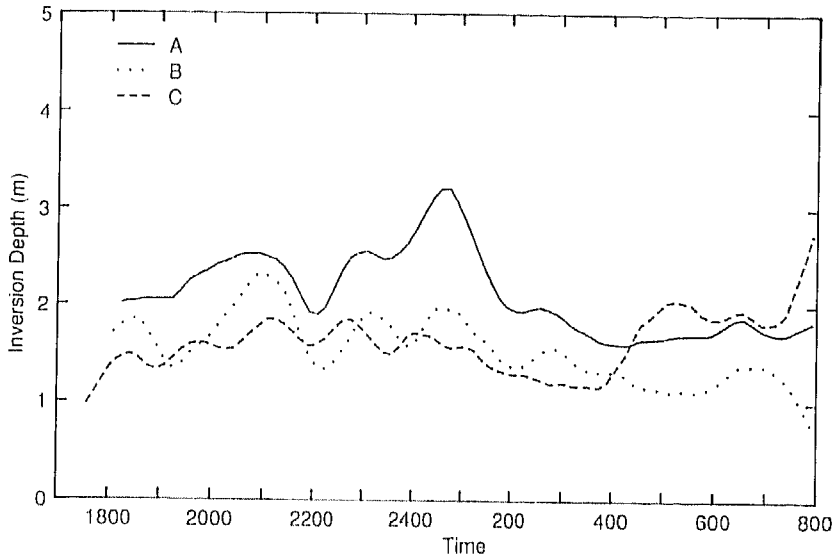

Fig. 12. Inversion depths at Towers A, B, and C on the night of 5–6 October.

decrease at tower C. The maximum strengths of the winds compare well with observations but fall off too rapidly with height. This could be caused by the neglect of ambient cross-valley winds that may be present. Even with this rapid decrease with height, the katabatic winds extend well beyond the 6-m height of the highest anemometers on the sidewalls. The inversion depth clearly decreases below tower A, and the inversion strength is noticeably smaller at tower C.

Although in Test 2 the inversion depth h decreased from tower A to C, the momentum depth h' increased by almost a factor of two. Thus, whereas the surface inversion became concentrated in a smaller depth (smaller h), the katabatic winds extended over a deeper layer (larger h'). This is a significant difference from the results over a simple slope with constant ambient stratification, where the two scales were closely related (Horst and Doran, 1986). It is not surprising, then, that in Table II the model predictions for a simple slope and the observations over valley sidewalls do not agree.

7. Summary and Conclusions

Perhaps the clearest impression produced by this study of slope flows in a simple valley is that their behavior is quite complex and not easily predicted by a few simple parameters. The development of katabatic flows on a valley sidewall was not readily inferred from studies of such flows on simple, isolated slopes, although

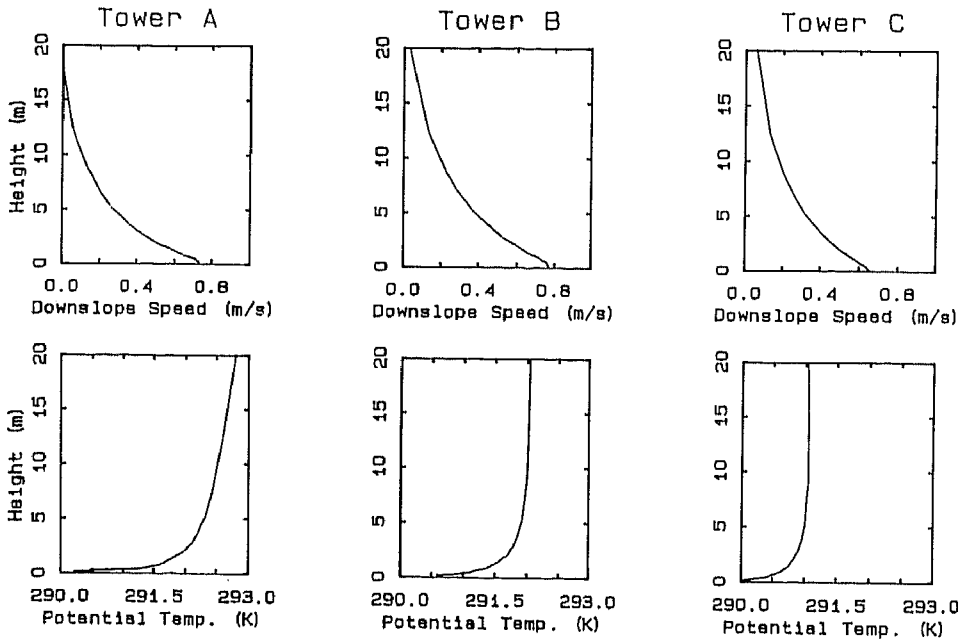

Fig. 13. Simulated wind and temperature profiles at Towers A, B, and C for Test 2 in Table IV.

such studies were quite useful in providing estimates of the relevant wind and temperature scales.

The detailed temperature structure of katabatic flows on valley sidewalls was found to be quite sensitive to the structure of the ambient temperature profile in the valley. However, the presence of cross-valley temperature gradients made it virtually impossible to define unambiguously an appropriate ambient temperature profile based on measurements in the valley center.

It is possible to characterize the temperature structure of slope flows in terms of two parameters, an inversion strength ΔT and an e-folding inversion depth h. After an initial transition period shortly after local sunset, the inversion depth on the east sidewall reaches a value on the order of 3 m in the upper third of the valley slope, and about 2 m in the lower half. These values usually decrease by about 1 m during the course of the night, with occasional increases of about 0.5 m in the lower third of the valley a few hours before sunrise. The inversion strength along the upper half of the slope typically peaks at values between 3 and 4 K during the transition period, and decreases to a value about one third as large later in the night. In the lower third of the valley, the inversion strength generally reaches a smaller peak value of about 1.4 K, which subsequently decreases to around 0.8 K.

Katabatically induced slope winds are generally weak, with measured peak values less than 1 m/s for most of the night. Observations and numerical simulations suggest that katabatic slope winds in this valley extend 10 m or more above the surface.

The ambient temperature profile in the valley frequently showed extended layers in which the potential temperature was constant. Observations and numerical simulations show that these layers are associated with decreases in the slope flow inversion depth scale h, but the numerical simulations also showed that this does not imply a decrease in the momentum depth scale, h'. Over simple slopes, the two depth scales will generally evolve similarly with downslope distance but in a valley this need not be true. The momentum depth, h', is difficult to define usefully or measure in the presence of ambient winds; in contrast, the inversion depth scale is less ambiguous and its behavior can be measured.

The model results also suggest that a proper description of the valley flow dynamics requires a detailed surface energy budget description to properly determine the lower boundary condition for the thermodynamic equation. Assumptions of constant cooling rates, constant temperature deficits, or sensible heat fluxes independent of downslope position are not supported by the data.

The role of the along-valley wind is also important. When the down-valley winds are weak, the integrated buoyancy deficit on the slopes can be large, and katabatic winds increase with increasing values of $h * \Delta T$. However, the development of strong down-valley flows produces enhanced mixing over the slopes, which limits the strength of the inversion that can develop there. Near the valley wind maximum, it can prevent a strong local inversion from ever forming on the sidewall.

Along the higher elevation slopes, the strength of the inversion that forms shortly after local sunset is subsequently reduced when the valley wind speeds increase. When the local sidewall inversions are only on the order of 1 to 2 K, the katabatic flows are weak, and the wind direction along the slopes is predominantly down-valley with a relatively small downslope component. Thus, the effects of the along-valley wind were at least as important as the valley inversion structure in determining the general features of katabatic flows on the slopes of a valley.

Acknowledgements

This research was supported by the U.S. Army Research Office under contract number DAAG29-K-0231. Additional support to deploy the Doppler sodar, to reduce the sodar data, and to develop the numerical model for slope flows was provided by the U.S. Department of Energy under contract DE-AC06-76RLO 1830. Mr. W. C. Pulliam, Mr. D. Rainwater, and Mr. W. Carlton, Jr. are thanked for permission to use their land and for their cooperation during the field measurement program. O. B. Abbey, G. W. Dennis, J. M. Hubbe, J. Buck, M. Schmeeckle, and D. Dovey assisted in setting up and maintaining the field equipment. J. M. Hubbe also assisted in data processing.

References

Brost, R. A. and Wyngaard, J. C.: 1978, 'A Model Study of the Stably Stratified Planetary Boundary Layer', *J. Atmos. Sci.* **35**, 1427–1440.

Brost, R. A. and Wyngaard, J. C.: 1979, 'Reply', *J. Atmos. Sci.* **36**, 1821–1822.

Doran, J. C. and Horst, T. W.: 1983, 'Observations and Models of Simple Nocturnal Slope Flows', *J. Atmos. Sci.* **40**, 708–717.

Filliger, P., Rickli, B., and Wanner, H.: 1987, 'Slope and Valley Wind Measurements and Their Comparison with Ambient Winds and Stability', in Preprints from the *Fourth Conference on Mountain Meteorology*, August 25–28, 1987, Seattle, Washington. Amer. Meteorol. Soc., Boston, Mass., pp. 70–75.

Horst, T. W. and Doran, J. C.: 1986, 'Nocturnal Drainage Flow on Simple Slopes', *Boundary-Layer Meteorol.* **34**, 263–286.

Horst, T. W. and Doran, J. C.: 1988, 'The Turbulence Structure of Nocturnal Slope Flow', *J. Atmos. Sci.* **45**, 605–616.

Manins, P. C. and Sawford, B. L.: 1979, 'A Model of Katabatic Winds', *J. Atmos. Sci.* **36**, 619–630.

Mellor, G. L. and Yamada, T.: 1982, 'Development of a Turbulence Closure Model for Geophysical Fluid Problems', *Rev. Geophys. Space Phys.* **20**, 851–875.

Nappo, C. J. and Rao, K. S.: 1987, 'A Model Study of Pure Katabatic Flows', *Tellus* **39A**, 61–71.

Prandtl, L.: 1942, "*Strömungslehre*' [Flow Studies]', Vieweg und Sohn, Braunschweig, 382 pp.

Whiteman, C. D.: 1986, 'Temperature Inversion Buildup in Colorado's Eagle Valley', *Meteorol. Atmos. Phys.* **35**, 220–226.